Improved Quasi-static Nodal Green's Function Method for cylindrical geometry

Zhenjia Gao, Fu Li, Yongming Hu
(Institute of Nuclear and New Energy Technology, Tsinghua University, Beijing, China 100084)

Abstract

Improved Quasi-static Nodal Green's Function Method for cylindrical geometry (IQS/CNGFM) is adopted to solve the multidimensional transient neutron diffusion equation. Numerical results demonstrate that the IQS/CNGFM method is feasible. Meanwhile, the paper provides the method to get physical adjoint flux and tests its calculation accuracy with definite differential method program CITATION to prove the method's feasibility.

Keywords: Improved Quasi-static Method Bessel Function Cylindrical Geometry Nodal Green's Function Method Physical Adjoint Flux

1. Introduction

The full scale simulator for High-temperature Gas-cooled Reactor (HTGR) is under development in the Institute of Nuclear and New Energy Technology, Tsinghua University. One of key technology for full scale simulator is to develop the fast physical dynamic calculation module. This physical dynamic module not only requires fast enough, but also can deal with the cylindrical geometry used in HTGR. Therefore, the Improved-quasi-static Cylindrical Nodal Green's Function Method (IQS/CNGFM) is proposed, implemented and validated in this paper.

In the IQS method[4], the neutron flux is factorized into amplitude and shape functions and the main change of neutron flux is concentrated on the amplitude function. Therefore, the most evident advantage of IQS method is that shape function can be determined by large time step. Furthermore, the spatial mesh-intervals can be enlarged based on nodal methods such as NGFM. So, the efficiency of the IQS/CNGFM is hopeful to meet the real-time demand of the simulator. What is more, the IQS/CNGFM method is developed under cylindrical geometry. CNGFM method[1] is derived on the basis of the Nodal Green's Function Method for Cylindrical Geometry on Neumann Boundary Condition. It is different from the presently broadly used code of Nodal Green's Function Method (NGFM) for neutron diffusion calculations under Cartesian geometry, which is based on the third kind boundary condition.

The formulation deduction for the IQS/CNGFM method transient neutron diffusion equations is carried out in Sec.2. One of prerequisite for IQS/CNGFM is the nodal adjoint flux under cylindrical geometry. So, in Sec.3., the process to calculate the physical nodal adjoint flux is evaluated. Through preliminary numerical verification, the IQS/CNGFM method is proven as feasible and reasonable. Finally, a brief discussion and conclusion is made in Sec.4.

2. Formulation of the method

The key idea of the IQS/CNGFM is that the neutron flux is factorized in product of an amplitude function and a shape function. It mainly consists of three steps as follows.

2.1 Factorization

The multi-dimensional transient neutron diffusion equation under cylindrical geometry can be written in standard multi –group form:

$$\begin{aligned}
&\frac{1}{V_g}\frac{\partial \Phi_g(r,\theta,z,t)}{\partial t} = \nabla\cdot D_g\nabla\Phi_g(r,\theta,z,t) - \Sigma_g^R\Phi_g(r,\theta,z,t) + \sum_{g'=1}^{g-1}\Sigma^s_{gg'}\Phi_{g'}(r,\theta,z,t) \\
&+(1-\beta)\chi_g\sum_{g'=1}^{G}\nu\Sigma_{fg'}\Phi_{g'}(r,\theta,z,t) + \chi_g\sum_{i=1}^{Id}\lambda_i C_i(r,\theta,z,t)(a) \\
&\frac{\partial C_i(r,\theta,z,t)}{\partial t} = \beta_i\sum_{g'=1}^{G}\nu\Sigma_{fg}\Phi_{g'}(r,\theta,z,t) - \lambda_i C_i(r,\theta,z,t)(b)
\end{aligned} \tag{1}$$

The parameters in the above equations are expressed with standard symbols. A factorization is introduced[2]:

$$\Phi_g(r,\theta,z,t) = n(t)*\Psi_g(r,\theta,z,t) \tag{2}$$

Where $\Psi_g(r,\theta,z,t)$ is time- and space-dependent shape functions, and n(t) represent their time-dependent amplitude functions. By substituting Eq.(2) into Eq.(1), the shape function equations can be obtained. That is

$$\begin{aligned}
&\frac{1}{V_g}\frac{\partial \Psi_g(r,\theta,z,t)}{\partial t} = \nabla\cdot D_g\nabla\Psi_g(r,\theta,z,t) - \Sigma_g^R\Psi_g(r,\theta,z,t) + \sum_{g'=1}^{g-1}\Sigma^s_{gg'}\Psi_g(r,\theta,z,t) \\
&+(1-\beta)\chi_g\sum_{g'=1}^{G}\nu\Sigma_{fg}\Psi_g(r,\theta,z,t) + \frac{\chi_g}{n(t)}\sum_{i=1}^{Id}\lambda_i C_i(r,\theta,z,t) - \frac{\Psi_g(r,\theta,z,t)}{V_g n(t)}\frac{\partial n(t)}{\partial t}(a) \\
&\frac{\partial C_i(r,\theta,z,t)}{\partial t} = n(t)*\beta_i\sum_{g'=1}^{G}\nu\Sigma_{fg}\Psi_g(r,\theta,z,t) - \lambda_i C_i(r,\theta,z,t)(b)
\end{aligned} \tag{3}$$

The multi-dimensional physical adjoint neutron diffusion equation under cylindrical geometry can be written in standard multi –group form:

$$-\nabla\cdot D_g\nabla\Phi^*_g(r,\theta,z) + \Sigma_g^R\Phi^*_g(r,\theta,z) = \sum_{g'=g+1}^{G}\Sigma^s_{g',g}\Phi^*_{g'}(r,\theta,z) + \frac{\nu\Sigma_{fg}}{k}\sum_{g'=1}^{G}\chi_{g'}\Phi^*_{g'}(r,\theta,z) \tag{4}$$

Eq.(4) can be solves as the steady multi-dimensional neutron diffusion equation to get the physical adjoint flux distribution.. Using the physical adjoint neutron of steady state $\phi^*_g(r,\theta,z)$ and $\chi_g\phi^*_g(r,\theta,z)$ as weight functions, Eq.(3) can be integrated over all space with a sum to all energy groups. Meanwhile, the shape functions should be constrained by introducing the normalization:

$$\sum_{g=1}^{G}\frac{1}{V_g}\int_V \phi^*_g(r,\theta,z)*\Psi_g(r,\theta,z,t)dv=1 \tag{5}$$

Then, the amplitude function is deduced.

$$\begin{aligned}\frac{\partial n(t)}{\partial t}&=\frac{\rho(t)-\bar{\beta}(t)}{\Lambda(t)}n(t)+\sum_{i=1}^{Id}\lambda_i\bar{C}_i(t)\\ \frac{\partial \bar{C}_i(t)}{\partial t}&=\frac{\bar{\beta}_i(t)}{\Lambda(t)}n(t)-\lambda_i\bar{C}_i(t)\end{aligned} \tag{6}$$

Where the parameters $\rho,\bar{\beta},\Lambda,\beta_i$, all are functions of $\Psi_g(r,\theta,z,t)$. Now, the shape function equations and amplitude function equations are deduced from Eq.(1).

2.2 Amplitude Function Equation

The amplitude function describes the fast evolution of the neutron flux. Its parameters can be determined as long as the time- and space-dependent shape distribution $\Psi_g(r,\theta,z,t)$ is known. Then, the shape function equations are equal to the 'point kinetic' equation, which possesse a property of stiffness in temporal domain. Because of the stiffness of the problem, the time steps for the solution of 'point kinetics' equations must be short enough to make the numerical calculations numerous stable. There are many kinds of approaches for the solution for the 'point kinetics' equations. In this paper, trapezoid formula is adopted because of its implicit time disposal and no need to iterate, although it indicates lower precision of computation and can not be suitable for the larger reactivity in the reactor, compared with other approaches such as Gear method and three-order Hermite polynomials method.

2.3 Shape Function Equation

The shape function accounts for the spatial distortions that takes place on a slower time scale. It is illustrated as follows.

$$\begin{aligned}&\frac{1}{V_g}\frac{\partial\Psi_g(r,\theta,z,t)}{\partial t}=\nabla\cdot D_g\nabla\Psi_g(r,\theta,z,t)-\Sigma_g^R\Psi_g(r,\theta,z,t)+\sum_{g'=1}^{g-1}\Sigma^s_{gg'}\Psi_g(r,\theta,z,t)\\ &+(1-\beta)\chi_g\sum_{g'=1}^{G}\nu\Sigma_{fg}\Psi_g(r,\theta,z,t)+\frac{\chi_g}{n(t)}\sum_{i=1}^{Id}\lambda_iC_i(r,\theta,z,t)-\frac{\Psi_g(r,\theta,z,t)}{V_g n(t)}\frac{\partial n(t)}{\partial t}(a)\\ &\frac{\partial C_i(r,\theta,z,t)}{\partial t}=n(t)*\beta_i\sum_{g'=1}^{G}\nu\Sigma_{fg}\Psi_g(r,\theta,z,t)-\lambda_iC_i(r,\theta,z,t)(b)\end{aligned} \tag{7}$$

Where the shape function is coupled with amplitude function by

$\frac{\chi_g}{n(t)}\sum_{i=1}^{Id}\lambda_i C_i(r,\theta,z,t)$ and $\frac{\Psi_g(r,\theta,z,t)}{V_g n(t)}\frac{\partial n(t)}{\partial t}$. In the paper, CNGFM method [5] is introduced to solve the shape function. Firstly, the 3-D neutron diffusion equation is converted into three coupled 1-D equations through a transverse integral as other advanced nodal methods. The expression for the corresponding Green's function with Neumann boundary condition is represented by a Bessel functions in the radial direction. The partial flux equations in the angular and axial directions are approximated in the form of slab geometry. Then all of the equations in the three directions are solved in the same way as in the Cartesian geometry. CNGFM method is capable to yield very accurate results in smaller computing time than those required by definite difference code CITATION[1].

3. Numerical results

3.1 Physical adjoint flux evaluation

New code to calculate the physical adjoint neutron flux distribution is developed on the basis of the CNGFM code. To validate the feasibility of IQS/CNGFM method, some numerical results are presented. Fig.1 shows the shape of the reactor. It consists of three regions-A is the reflector, B is the region with control rods and C is the fuel region. Table 1 is the cross sections of each region. The reference solution of this model is obtained by CITATION.

Table 2 demonstrates that the Keff calculated by CNGFM method has high precision according to reference result of fine mesh with CITATION. Table 3 shows that the relative errors of adjoint flux distributions exist in region B and C. It indicates that the highest relative error is smaller than 0.1% in region C and smaller than 0.5% in region B. In region A, the relative errors increase, which are illustrated in Fig.2. However, only the outside ring with about 15cm-width has the relative error larger than 10%. It nearly has no influence on the dynamic calculation as a weight function because the neutron flux in this region is almost zero.

Figure 1: Reactor model

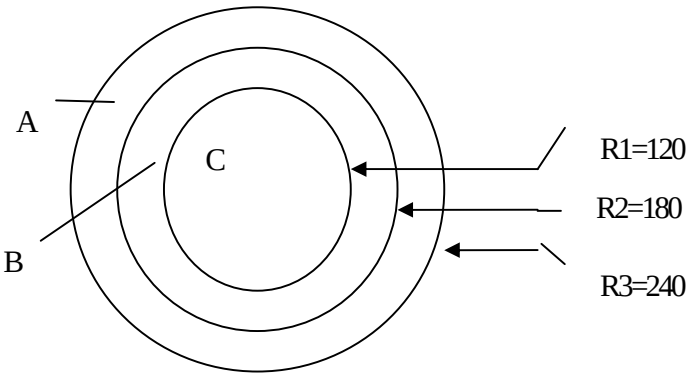

Table 1: Cross sections

material	Energy (g)	D(cm)	$\Sigma_a(cm^{-1})$	$\Sigma_f(cm^{-1})$	$\nu\Sigma_f(cm^{-1})$	$\Sigma_{s,g\to g+1}(cm^{-1})$
A	1	1.85540E+00	1.73498E-05	0.00000E+00	0.00000E+00	1.28846E-02
	2	9.96964E-01	1.00000E-05	0.00000E+00	0.00000E+00	6.83588E-03
	3	9.84588E-01	2.85612E-05	0.00000E+00	0.00000E+00	2.07258E-02
	4	9.81092E-01	2.97593E-04	0.00000E+00	0.00000E+00	0.00000E+00
B	1	2.22361E+00	1.44768E-05	0.00000E+00	0.00000E+00	1.07510E-02
	2	1.19482E+00	2.59984E-06	0.00000E+00	0.00000E+00	5.70391E-03
	3	1.17998E+00	2.38318E-05	0.00000E+00	0.00000E+00	1.72938E-02
	4	1.17579E+00	1.00000E-02	0.00000E+00	0.00000E+00	0.00000E+00
C	1	2.85717E+00	2.62273E-05	1.03437E-05	2.69980E-05	9.00545E-03
	2	1.64564E+00	2.24884E-04	6.47316E-05	1.57751E-04	4.59003E-03
	3	1.62395E+00	1.09501E-03	2.03076E-04	4.94830E-04	1.40918E-02
	4	1.58940E+00	1.59195E-03	1.21260E-03	2.95474E-03	0.00000E+00

Table 2: The K_{eff} calculated by CNGFM and CITATION

	CNGFM	CITATION	Relative error (%)
K_{eff}	1.08938839	1.0895060	0.01

Table 3 : Relative error of adjoint flux in region B and C

	region	1group	2group	3group	4group
Highest relative error	C	4.30E-04	3.88E-04	-4.91E-04	-1.00E-03
	B	-7.76E-04	-1.20E-03	-3.68E-03	-4.19E-03

Figure 2: Relative error in region A

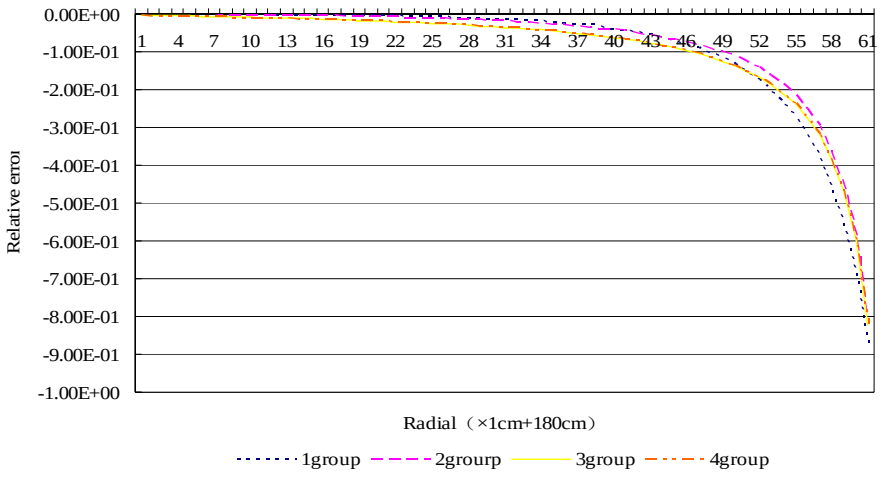

3.2 R-Model

The reactor model and cross sections are illustrated in Sec.3.1. The steady Keff is 1.08938629, which is used to divide production section to make the unperturbed reactor exhibit a steady state transient behavior. Then, change the absorption section of group 4 in region C from 1.59195E-03 cm-1 to 1.59677585E-03cm-1 linearly in the first two seconds. A minus reactivity is introduced at this time; then change the same section to decrease to 1.59677585E-03 cm-1 in the following 2 seconds. This course is to simulate the effect of inserting control rods. A positive reactivity is introduced at this time. The reactor power change is illustrated in Fig.3.

Figure 3: Total reactor power

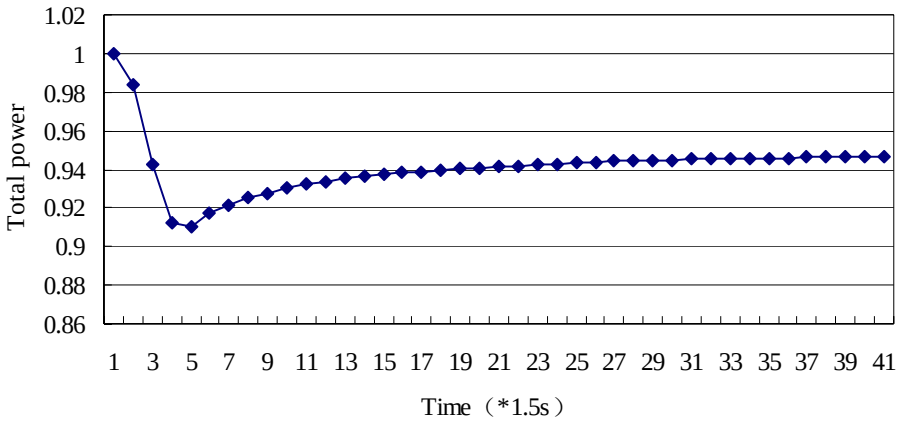

Fig.3 demonstrates that the reactor power decreases when the negative reactivity is induced in the beginning. After 3 seconds, it keeps decreasing although the absorption section of group 4 decreases, because the flux distribution change slowly and the reactivity can not increase immediately. At about 5 seconds, the power begins to increase to steady state slowly.

3.3 R-Z Benchmark model

The reactor model is as follows. (1) and (2) are the top reflectors. (14) and (15) are the bottom reflectors. The regions with the numbers from (3) to (13) and (16) are fuel regions. Other parameters of this reactor are listed in reference 3.

Initiating Perturbation:

In regions 3 and 7,

$$\Sigma_2(t) = (1 + 0.03t)\ \Sigma_2(0), t < 1$$
$$\Sigma_2(t) = 1.03\Sigma_2(0), t \geq 1, t = time(\text{sec})$$

In region 11,

$$\Sigma_2(t) = (1-0.03t)\ \Sigma_2(0), t < 1$$
$$\Sigma_2(t) = 0.97\Sigma_2(0), t \geq 1, t = time(\text{sec})$$

Where Σ_2 is the absorption section of group 2.

Figure 4: R-Z Benchmark model

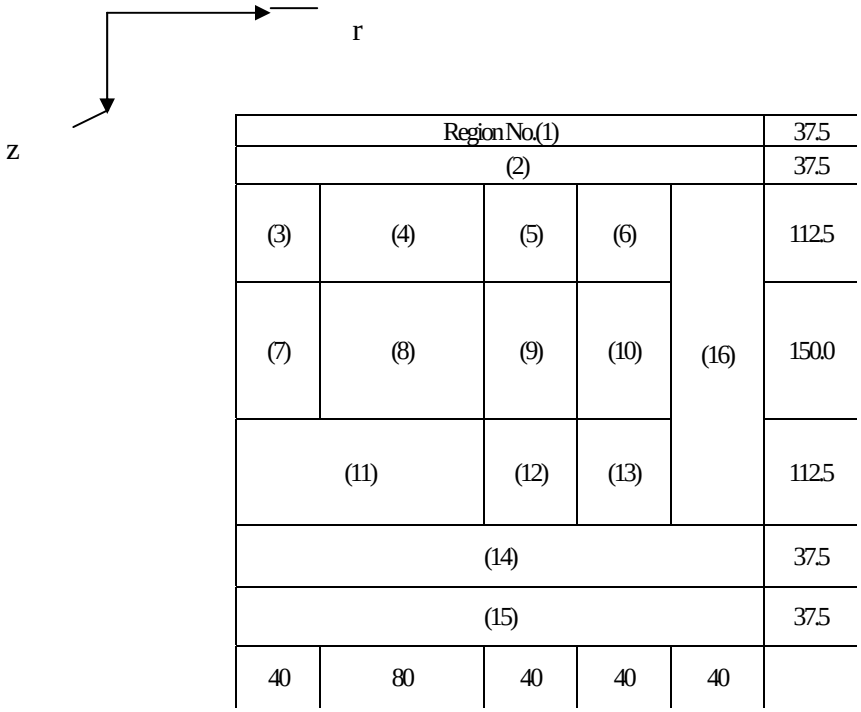

In region 3 and 7, a negraive reactivity is introduced while a positive reactivity is introduced in region 11 at the same time. So, the extent of the distortion of neutron flux is very large.

The reference benchmark calculation[3] adopts a 5-points difference approximation. The time step is △t=0.001s and the space interval is △R=8cm, △z=18.75cm. The time step of IQS/CNGFM is △t=1.0s and the space interval is the same as the benchmark model. The reference Keff is 0.86705 while that of IQS/CNGFM is 0.86720085. Therefor, the precision is 1.71E-4.

The reactor power change in the first 4 seconds is as follows.

Table 4: total power versus time as function of time-step size

time	difference	IQS/CNGFM	Relative error
0	1.000	1.000	0
1.0	1.596	1.595	-0.00063
2.0	2.027	1.856	-0.08436
3.0	2.335	2.085	-0.10707
4.0	2.659	2.570	-0.03347

The paper considers the errors owing to two reasons. First, the precision of trapezoid formula is somewhat low. Second, in fact, the reactivity introduced in the reactor changes along with time, but IQS method supposes it keep stable in the micro time step and reactivity time step by jump. The relative error of relative power density averaged over height and radius is illustrated in table 5.

Table 5: the relative error of relative power density averaged over height and radius

radius				axial			
Radius (cm)	t=0s	t=1s	t=4s	Height (cm)	t=0s	t=1s	t=4s
8	-0.05093	-0.05305	-0.08669	18.75	——	——	——
16	-0.0514	-0.04394	-0.07815	37.5	——	——	——
24	-0.05153	-0.03886	-0.07304	56.25	——	——	——
32	-0.05096	-0.04622	-0.07972	75	——	——	——
40	-0.0511	-0.05083	-0.08409	93.75	-0.00125	-0.13165	-0.13947
48	-0.05136	-0.04954	-0.08273	112.5	-0.03604	-0.03767	-0.04695
56	-0.0512	-0.04775	-0.08112	131.25	-0.05102	-0.00632	-0.01713
64	-0.05166	-0.04942	-0.08225	150	-0.05933	0.003762	-0.00908
72	-0.05143	-0.05099	-0.08383	168.75	-0.06564	0.005946	-0.00846
80	-0.05127	-0.05253	-0.08506	187.5	-0.06419	0.009461	-0.00798
88	-0.0516	-0.05344	-0.08565	206.25	-0.06234	-0.01162	-0.03158
96	-0.05117	-0.0534	-0.08547	225	-0.06503	-0.03762	-0.06051
104	-0.0511	-0.05291	-0.08445	243.75	-0.06637	-0.05902	-0.0849
112	-0.05107	-0.05114	-0.08264	262.5	-0.06665	-0.07687	-0.10579
120	-0.05286	-0.04982	-0.08105	281.25	-0.06637	-0.09266	-0.12437
128	-0.04904	-0.04612	-0.07734	300	-0.06503	-0.10706	-0.1412
136	-0.04517	-0.04406	-0.07488	318.75	-0.06234	-0.12054	-0.15706
144	-0.04238	-0.04186	-0.07242	337.5	-0.06419	-0.1367	-0.17447
152	-0.03754	-0.0375	-0.06838	356.25	-0.06564	-0.12322	-0.16328
160	-0.03113	-0.03123	-0.06214	375	-0.05933	-0.09794	-0.14027
168	-0.02347	-0.02411	-0.05523	393.75	-0.05102	-0.06586	-0.1109
176	-0.01945	-0.02096	-0.052	412.5	-0.03604	-0.01177	-0.06003
184	-0.01237	-0.01507	-0.04587	431.25	-0.00125	0.114147	0.059424
192	0.00122	-0.00132	-0.03224	450	——	——	——
200	-0.00859	-0.01048	-0.04195	468.75	——	——	——
208	0.053035	0.048433	0.015895	487.5	——	——	——
216	0.072674	0.068931	0.035276	506.25	——	——	——

Table 5: The relative error of relative power density averaged over height and radius

224	0.131855	0.127853	0.092744	525	——	——	——
232	0.264505	0.336023	0.292961	——			
240	——	——	——				

The convergence precision is not very high in the iteration, so the relative errors in table 5 are not accurate. In the reactor, except region (1),(2),(14),(15) and (16), the largest relative error distribution is listed in table 6.

Table 6: Relative error in inner reactor

Time	Radial		Axial	
	Relative error	Location(cm)	Relative error	Location(cm)
0s	5.286E-2	120	6.665E-2	262.5
1s	5.344E-2	88	>10%	Region among 11,7,8
4s	8.565E-2	88	>10%	Region among 11,7,8

In the inner of the reactor core, the largest relative error is located where the distortion of the neutron flux is very large. The neutron flux distribution change along time can not be considered in linearity in these areas within the shape function time step and should be replaced by other model.

In the outer of reactor, region 1, 2, 14, 15 and 16, the relative errors are larger than those of the inner reactor, because of the transverse integral in CNGFM method. In the inner reactor, the neutron flux can be factorized as the product of axial cosine function and radial Bessel Function accurately. But in the outer reactor, this factorization will introduce large error. Small mesh intervals in outer reactor should be helpful to reduce error. The radial and axial relative power distributions are demonstrated in Fig. 6 and Fig.7.

Figure5: Relative axial power distribution

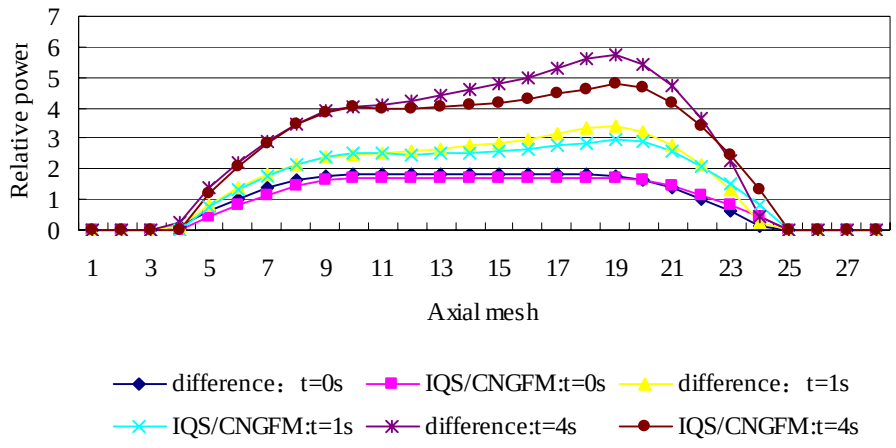

Figure 6: Relative radial power distribution

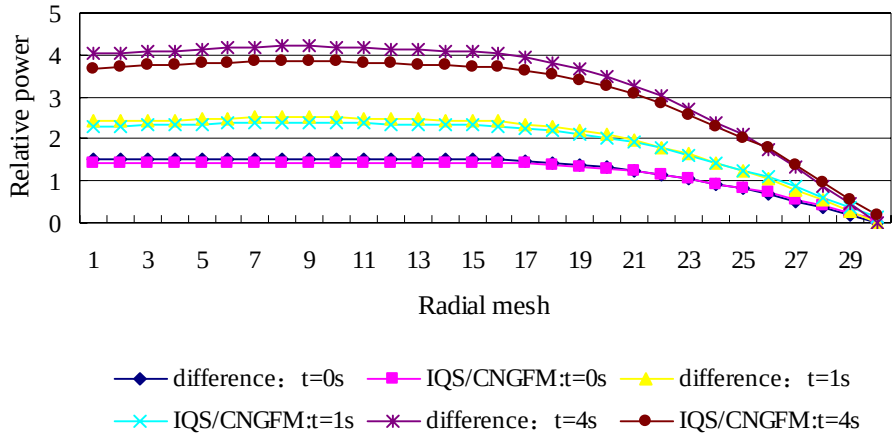

4. Conclusion

A nodal method coupled with improved quasi-static method for the solution of multidimensional kinetic problems in cylindrical geometry has been presented and numerical tested in the paper. The results show that IQS/CNGFM approach is a feasible method for cylindrical reactor's dynamic simulation. It provided good basis for building the fast physical simulation module for HTGR full scale simulator, although it should be improved in many aspects, such as iteration techniques, benchmark problem verification, real time technology, coupling with other modules, and etc.

Acknowledgements

Thank the editors of PHYSOR 2004 for the original version of this paper.

References

1) Qinxing Du, "The Nodal Green's Function Method For Cylindrical Geometry on Neumann Boundary Condition Based on Bessel Function", Doctor Thesis, Department of Engineering Physics, Tsinghua University, 2000
2) Junli Li, "Improved quasi-static Green's Function method", Doctor Thesis, Department of Engineering Physics, Tsinghua University, 1994
3) Argonne National Laboratory, "Argonne Code Center: Benchmark Problem Book", ANL~7416 Supplement 2, 1977, 182~269
4) Jing Xingqing, Li Junli, and Hu Dapu, "Improved quasi-static nodal Green's function method", Nulear science and techniques, 7, 2 (1995), 90~94
5) Du Qixin, Shi Gong, Hu Yongming, "Nodal Green's function method for 3-D cylindrical geometry", J Tsinghua Univ (Sci & Tech), 41, 4/5 (2001), 13~16
6) Hu Yongming, Zhao Xianfeng, "Advanced nodal Green's function method on Neumann boundary condition", [J]. J Tsinghua Univerdity, 38, 4 (1998), 17~21